

Electronegative S/Se co-filled and Fe-substituted p-type skutterudites prepared by high-temperature and high-pressure technique

Xiaoxu Kang(康晓旭), Hongan Ma(马红安), Xin Fan(范鑫), Mingye Sun(孙明烨), Guihong Zuo(左桂鸿), and Youjin Zheng(郑友进)

Citation: Chin. Phys. B, 2026, 35 (**8**): 087201. DOI: 10.1088/1674-1056/ae77d4
http://cpb.iphy.ac.cn; http://iopscience.iop.org/cpb

What follows is a list of articles you may be interested in

Reducing lattice thermal conductivity via phonon engineering: Strategies for high-performance thermoelectrics

Yayu Wang(王亚雨), Jue Hou(侯爵), Ming Yang(杨明), and Xingli Zhang(张兴丽)
Chin. Phys. B, 2026, 35 (**3**): 037201. DOI: 10.1088/1674-1056/ae1c22

Realize high thermoelectric performance in both zone-melted ingots and powder-metallurgy bulks of $Bi_{0.46}Sb_{1.54}Te_3$

Kai-Wen Zhao(赵凯雯), Meng-Yao Li(李梦瑶), Ying-Jiu Zhang(张迎九), and Hong-Zhang Song(宋红章)
Chin. Phys. B, 2025, 34 (**10**): 107203. DOI: 10.1088/1674-1056/add503

High thermoelectric performance of SnS under high pressure and high temperature

Yuqi Gao(高语崎), Xinglin Wang(王星淋), Cun You(由存), Dianzhen Wang(王殿振), Nan Gao(高楠), Qi Jia(贾琪), Zhihui Li(李志慧), Qiang Tao(陶强), and Pinwen Zhu(朱品文)
Chin. Phys. B, 2025, 34 (**8**): 087201. DOI: 10.1088/1674-1056/addbc8

High-entropy alloys in thermoelectric application: A selective review

Kai Ren(任凯), Wenyi Huo(霍文燚), Shuai Chen(陈帅), Yuan Cheng(程渊), Biao Wang(王彪), and Gang Zhang(张刚)
Chin. Phys. B, 2024, 33 (**5**): 057202. DOI: 10.1088/1674-1056/ad34c5

Synthesis and thermoelectric properties of Nd-single filled p-type skutterudites

Hong Wu(吴宏), Nusrat Shaheen, Heng-Quan Yang(杨恒全), Kun-Ling Peng(彭坤岭), Xing-Chen Shen(沈星辰), Guo-Yu Wang(王国玉), Xu Lu(卢旭), Xiao-Yuan Zhou(周小元)
Chin. Phys. B, 2018, 27 (**4**): 047203. DOI: 10.1088/1674-1056/27/4/047203

Electronegative S/Se co-filled and Fe-substituted p-type skutterudites prepared by high-temperature and high-pressure technique

Xiaoxu Kang(康晓旭)[1], Hongan Ma(马红安)[2], Xin Fan(范鑫)[1], Mingye Sun(孙明烨)[1,†], Guihong Zuo(左桂鸿)[1,‡], and Youjin Zheng(郑友进)[1]

[1] *School of Physics and Electronic Engineering, Mudanjiang Normal University, Mudanjiang* 157011, *China*
[2] *State Key Laboratory of Superhard Materials, College of Physics, Jilin University, Changchun* 130012, *China*

(Received 24 April 2026; revised manuscript received 30 May 2026; accepted manuscript online 4 June 2026)

Although n-type skutterudites modified by electropositive fillers have been extensively studied, research on p-type skutterudites filled with electronegative elements remains scarce. In this work, a series of sulfur/selenium (S/Se) co-filled and iron (Fe)-doped p-type skutterudite samples with a nominal composition of $S_{0.1-x}Se_xFe_{0.2}Co_{3.8}Sb_{12}$ ($x = 0.025$, 0.05, 0.075, 0.1) were rapidly synthesized via the high-temperature and high-pressure (HPHT) technique. Phase analysis indicates that the as-prepared samples possess a pure skutterudite structure without obvious impurity phases. Microstructural observations demonstrate that S/Se co-filling can effectively regulate the grain morphology and the evolution of grain size. Electrical transport measurements reveal that Fe substitution successfully induces p-type conductivity and optimizes the carrier transport behavior. Meanwhile, S/Se co-filling introduces strong phonon scattering, which significantly reduces the lattice thermal conductivity. For the optimal $S_{0.075}Se_{0.025}Fe_{0.2}Co_{3.8}Sb_{12}$, fitting based on the Debye–Callaway model confirms that the resonant frequencies of S and Se are 43.96 cm^{-1} and 35 cm^{-1}, respectively. Finally, the $S_{0.075}Se_{0.025}Fe_{0.2}Co_{3.8}Sb_{12}$ sample achieves a maximum zT value of approximately 0.22 at 673.15 K. This study provides a feasible strategy for constructing electronegative element co-filled p-type skutterudites and deepens the understanding of multiscale phonon scattering mechanisms in thermoelectric materials.

Keywords: S/Se co-filling, skutterudites, thermoelectric materials, high-temperature and high-pressure

PACS: 72.15.Jf, 72.20.Pa, 72.20.–i, 07.35.+k

DOI: 10.1088/1674-1056/ae77d4 **CSTR:** 32038.14.CPB.ae77d4

1. Introduction

In the face of intensifying global energy shortages and environmental challenges, the enhancement of energy utilization efficiency and the high-yield recovery of waste heat have become issues of crucial importance.[1,2] In this context, thermoelectric materials, which offer the capability for direct conversion of waste heat into electrical energy, have attracted considerable research interest. The performance of thermoelectric materials is quantitatively assessed by the dimensionless figure of merit, denoted as zT:

$$zT = \frac{S^2\sigma T}{\kappa}, \tag{1}$$

where S corresponds to the Seebeck coefficient, σ corresponds to the electrical conductivity, T corresponds to the absolute temperature, and κ corresponds to the thermal conductivity.[3] Improving the conversion efficiency requires an enhancement of the power factor (PF $= S^2\sigma$) in thermoelectric materials, concurrently with a reduction in thermal conductivity, presenting a substantial challenge for synergistic optimization.

Since the introduction of the phonon glass-electron crystal (PGEC) concept by Slack in 1995,[4] skutterudite has been extensively investigated as a leading candidate for thermoelectric applications in the mid-temperature regime (500–800 K), attributed to its body-centered cubic cage structure (space group $Im\bar{3}$) and considerable potential for property modulation.[4,5] Binary $CoSb_3$, the prototypical skutterudite compound, exhibits excellent electrical transport performance, including high electron mobility, along with low cost and environmentally benign constituents. The intrinsic lattice voids (2*a* sites) within the crystal structure can accommodate guest filler atoms, and multi-element substitution can be realized at Co or Sb sites, thereby providing a flexible structural foundation for the synergistic optimization of thermoelectric performance.[1] However, the material's relatively high lattice thermal conductivity (7 $W{\cdot}m^{-1}{\cdot}K^{-1}$) substantially limits its energy conversion efficiency, constituting a major obstacle for practical implementation. At present, the primary strategies for reducing the thermal conductivity of $CoSb_3$ include cage-site filling, substitution at matrix atomic sites, and nanostructuring. Among these, cage-site filling is considered the most consistent with the PGEC principle, as it concurrently facilitates enhanced phonon scattering and effective modulation of charge carriers. Electropositive elements such as Ce, Yb, Ba, and Ca tend to lose electrons.[6–9] When incorporated into the intrinsic lattice voids, these elements donate carriers to the ma-

†Corresponding author. E-mail: sunmingye203@126.com
‡Corresponding author. E-mail: zuoguihongmsy@163.com

© 2026 Chinese Physical Society and IOP Publishing Ltd. All rights, including for text and data mining, AI training, and similar technologies, are reserved.

trix. Meanwhile, their localized vibrations within the voids significantly reduce the lattice thermal conductivity. Such filling modification techniques are relatively mature, and early research mainly focused on the fabrication and performance optimization of n-type skutterudites, with rare earths and alkaline earth metals widely employed as fillers.[10–12] In contrast, the filling of electronegative elements (S, Se, Cl, Br, I, F) has attracted research attention only in recent years.[13–18] Such modification normally requires site substitution to realize charge compensation, and is mostly adopted to construct high-performance n-type skutterudites.[17,19–23] Up to now, systematic studies on electronegative-element-filled p-type skutterudites remain relatively scarce.

This study focuses on p-type skutterudite materials filled with electronegative elements. A synergistic modification strategy involving S/Se double filling and Fe substitution is employed. A series of S/Se double-filled and Fe-substituted skutterudite samples, denoted as $S_{0.1-x}Se_xFe_{0.2}Co_{3.8}Sb_{12}$, are synthesized via a high-temperature and high-pressure (HPHT) technique. Experimental results demonstrate that S/Se double filling regulates grain morphology and enhances phonon scattering, while Fe substitution enables p-type conduction and optimizes electrical transport properties. Fitting based on the Debye model indicates that point defect scattering is the dominant mechanism for reducing lattice thermal conductivity, with the resonant frequencies of S/Se double filling being 43.96 cm^{-1} and 35 cm^{-1}, respectively. Consequently, $S_{0.075}Se_{0.025}Fe_{0.2}Co_{3.8}Sb_{12}$ achieves a peak zT of approximately 0.22 at 673.15 K, offering a new pathway for optimizing the performance of p-type skutterudites.

2. Experiment and characterization

2.1. Experimental detials

High-purity sulfur (S) powder, selenium (Se) powder, iron (Fe) powder, cobalt (Co) powder, and antimony (Sb) powder served as the raw materials, with their detailed specifications as follows: S powder (purity 99.5%, Aladdin), Se powder (purity 99.99%, Aladdin), Fe powder (purity 99.95%, Aladdin), Co powder (purity 99.9%, Aladdin), and Sb powder (purity 99.9%, Aladdin). These powders were meticulously weighed and subsequently blended in accordance with the targeted nominal stoichiometric ratios corresponding to $S_{0.1-x}Se_xFe_{0.2}Co_{3.8}Sb_{12}$ ($x = 0.025$, 0.05, 0.075, 0.1). Following this, the mixed powders were ground in an agate mortar and cold-pressed into cylindrical pellets with dimensions of 10.5×4 mm (diameter $\times$ height). The cold-pressed pellets were then wrapped in molybdenum foil to prevent contamination during the subsequent HPHT process, and the wrapped cylindrical compacts were assembled in the sequence depicted in Fig. 1. Subsequently, the fully assembled block was transferred into the cavity of a China-style large-volume cubic high-pressure apparatus (CHPA, model SPD6 $\times$ 1400) for HPHT synthesis. The HPHT synthesis conditions were fixed as follows: a pressure of 3.0 GPa, a temperature of 900 K (627 °C), and a holding time of 30 minutes. Heating inside the cavity was achieved by passing an electric current through a graphite tube, while the pressure was controlled via a hydraulic anvil system. The temperature inside the cavity was monitored using a double platinum–rhodium thermocouple; calibration measurements were performed at different heating powers to establish the temperature profile and calibrate the internal temperature of the cavity. Additionally, the pressure inside the cavity was calibrated against the oil pressure using standard materials (Ba, Bi, Tl) with known phase-transition points. Through these procedures, skutterudite samples were successfully synthesized.

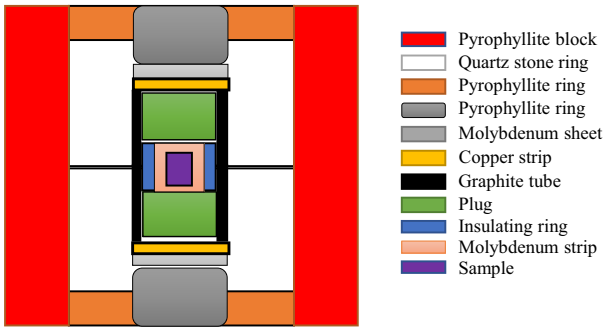


Fig. 1. Sample assembly diagram.

2.2. Characterization

The phase composition of the samples was analyzed by x-ray diffraction (XRD) using a Rigaku D/2550 V/PC diffractometer (Japan) with Cu-$K\alpha$ radiation ($\lambda = 0.15418$ nm). The measurements were performed at 40 kV and 200 mA over a 2θ range from 20° to 80°, with a scanning speed of 4°/min and a step size of 0.02°. The fracture morphology and grain orientation of the samples were characterized by field emission scanning electron microscopy (SEM, Hitachi S-4800) at an accelerating voltage of 5 kV. The as-prepared sample with a diameter of 10.5 mm and length of 4 mm was cut into two standard test pieces using an STX-202A wire-cutting machine: a rectangular bar of 2 mm×2 mm×8 mm and a cylindrical disk with a diameter of 10.5 mm and thickness of 2 mm. After cutting, the surfaces of all samples were polished to remove machining damage. The Seebeck coefficient (S) and electrical conductivity (σ) were measured simultaneously on the rectangular bar samples from 323 K to 773 K using a Namicro-3L variable-temperature thermoelectric measurement system (JouleYacht, China) under a helium atmosphere. The thermal diffusivity (α) of the disk samples was tested using the laser flash method (Netzsch LFA 467, Germany) over the same temperature range. Both sides of the disk samples were sprayed

with graphite to improve measurement accuracy. The total thermal conductivity κ was calculated using the following relation:

$$\kappa = \lambda C_{\mathrm{p}} D, \tag{2}$$

where D is the sample density measured by the Archimedes method with anhydrous ethanol as the immersion medium, and C_{p} is the specific heat capacity estimated according to the Dulong–Petit law.

2.3. Computational details

The first-principles calculations in this work were performed using the Vienna *Ab initio* Simulation Package (VASP) based on density functional theory (DFT) with the Perdew–Burke–Ernzerhof (PBE) functional within the generalized gradient approximation (GGA). The projector-augmented wave (PAW) method was employed, with a plane-wave cutoff energy of 450 eV. A 2×2×2 supercell was constructed, and convergence tests of the total energy were carried out under different pressures. A Γ-centered 5×5×5 k-point mesh was adopted for Brillouin zone sampling. To ensure the accuracy of structural optimization, the convergence criteria for energy and force were set to 1×10^{-6} eV/atom and 0.01 eV/Å, respectively.

3. Results and discussion

Figure 2 displays the XRD patterns of the $S_{0.1-x}Se_xFe_{0.2}Co_{3.8}Sb_{12}$ ($x = 0.025, 0.05, 0.075, 0.1$) samples synthesized at 3.0 GPa. As illustrated in Fig. 2(a), all major diffraction peaks can be well indexed to the cubic skutterudite phase with the $Im\bar{3}$ space group (JCPDS PDF#78-0977). No detectable secondary phases, such as impurity antimonides or elemental Sb, are observed across the entire composition range, confirming the formation of single-phase solid solutions and the homogeneous incorporation of S/Se co-filling and Fe doping into the skutterudite framework under the applied high-pressure conditions.

Figure 3 shows the cross-sectional SEM images of the S/Se double-filled Fe-substituted skutterudite samples synthesized at 3.0 GPa. As shown in Fig. 3(a) ($x = 0.025$), the sample with the lowest Se content possesses relatively large grains. In contrast, Fig. 3(b) ($x = 0.05$) shows significant grain refinement, presenting the finest and most uniform grain size distribution among all compositions. With further increasing Se content, Fig. 3(c) ($x = 0.075$) and Fig. 3(d) ($x = 0.1$), the highest Se content exhibits a gradual grain coarsening behavior. In the filled skutterudite system, both S and Se atoms occupy the intrinsic cages of the skutterudite lattice, but their different migration behaviors and interactions with the $CoSb_3$ framework dominate the grain growth kinetics.[24] At low Se content, the introduction of Se atoms induces lattice strain and suppresses grain growth, leading to refined grains. With increasing Se content, enhanced atomic diffusion and recrystallization promote grain coarsening.[25] This trend confirms that the co-filling of S and Se effectively modulates the microstructure of the skutterudite matrix, which is favorable for tailoring the thermoelectric properties.

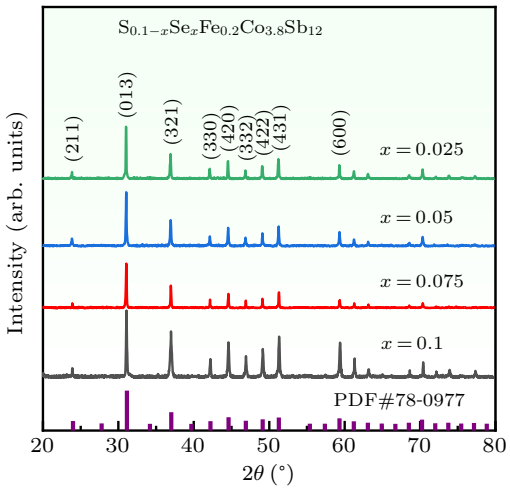


Fig. 2. XRD spectra of S/Se double filled Fe substituted skutterudite samples at HPHT.

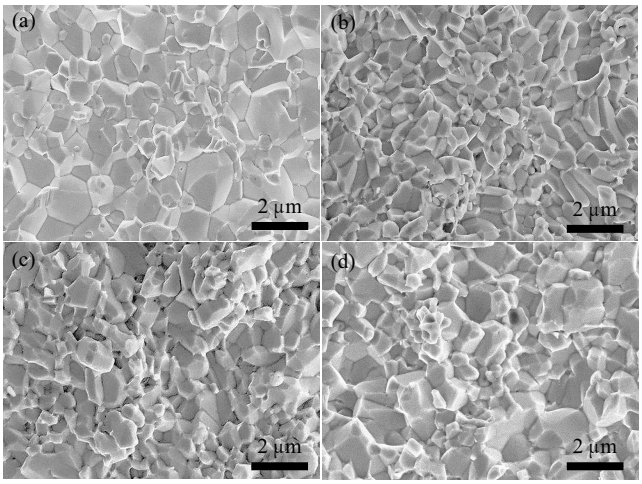


Fig. 3. SEM of $S_{0.1-x}Se_xFe_{0.2}Co_{3.8}Sb_{12}$ samples: (a) $x = 0.025$, (b) $x = 0.05$, (c) $x = 0.075$, (d) $x = 0.1$.

Figure 4 presents the temperature-dependent electrical properties of the $S_{0.1-x}Se_xFe_{0.2}Co_{3.8}Sb_{12}$ samples synthesized at 3.0 GPa. As shown in Fig. 4(a), the electrical conductivity (σ) of all samples exhibits a typical behavior of first increasing and then decreasing with rising temperature. At 323 K, the conductivity varies with Se content, showing a trend of increasing first and then decreasing, with the maximum value of 3.77×10^4 S·m^{-1} achieved by the sample with $x = 0.75$ ($S_{0.025}Se_{0.075}Fe_{0.2}Co_{3.8}Sb_{12}$). This temperature dependence is characteristic of heavily doped semiconductors, where the increase in carrier concentration dominates at low temperatures, while enhanced phonon scattering leads to a decrease in mobility at high temperatures.[26] Figure 4(b) shows

the temperature dependence of the Seebeck coefficient (S). All samples exhibit positive Seebeck coefficients, confirming their p-type conduction behavior. The Seebeck coefficient of each sample first increases with temperature and then decreases at higher temperatures, which is attributed to the onset of bipolar diffusion.[19] A maximum Seebeck coefficient of 132.24 $\mu V \cdot K^{-1}$ is observed at 623 K for the $x = 0.025$ sample. These results demonstrate that the S/Se co-filling effectively modulates both the carrier concentration and scattering mechanism, providing an opportunity to optimize the thermoelectric performance of the skutterudite system.

To qualitatively understand the effect of S/Se co-filling on the band structure, DFT calculations were performed on simplified model compositions with higher filling fractions ($Se_{0.5}S_{0.5}FeCo_7Sb_{24}$ and $SeFeCo_7Sb_{24}$), which preserve the essential electronic features. Figure 4(c) shows the calculated band structures of $Se_{0.5}S_{0.5}FeCo_7Sb_{24}$ (green curves) and $SeFeCo_7Sb_{24}$ (black curves). For the p-type skutterudite system in this study, the non-degenerate Boltzmann approximation is no longer applicable. Based on the degenerate parabolic band model, the Seebeck coefficient of a p-type semiconductor can be expressed as[27,28]

$$S = \frac{\pi^2 k_B^2 T}{3e}\left(r + \frac{3}{2}\right)\frac{1}{E_v - E_F}, \tag{3}$$

where S is the Seebeck coefficient, k_B is the Boltzmann constant, e is the elementary charge, E_v is the valence band maximum energy, E_F is the Fermi level energy, and r is the scattering factor. For the p-type skutterudite system, phonon scattering is the dominant scattering mechanism, and thus $r = -1/2$. Under identical temperature and scattering conditions, the S is inversely proportional to the energy difference between the valence band maximum and the Fermi level ($E_v - E_F$). For the S/Se co-filled $Se_{0.5}S_{0.5}FeCo_7Sb_{24}$ at a given doping level, the Fermi level lies closer to the valence band maximum, leading to a smaller $E_v - E_F$, which theoretically results in a larger S. This trend is also consistent with the Seebeck coefficient data shown in Fig. 4(b), where the sample with the lowest Se content ($x = 0.025$, corresponding to the S/Se co-filled case) exhibits the highest S values.

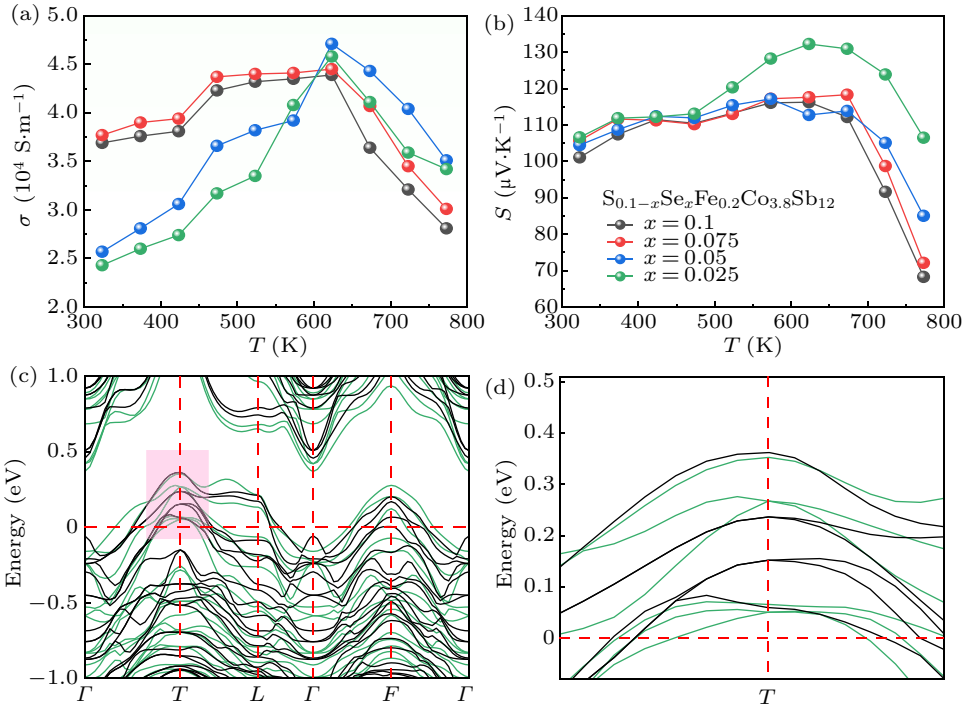


Fig. 4. Temperature dependence curve of electrical properties of S/Se double filled Fe substituted skutterudite samples: (a) conductivity, (b) Seebeck coefficient. (c) Band structures at 3.0 GPa: $Se_{0.5}S_{0.5}FeCo_7Sb_{24}$ (green curves) and $SeFeCo_7Sb_{24}$ (black curves). (d) Magnified view of the band region near the Fermi level marked in (c).

Figure 5 presents the thermal transport properties of the $S_{0.1x}Se_xFe_{0.2}Co_{3.8}Sb_{12}$ samples synthesized at 3.0 GPa. The thermal conductivity of a material consists of two components: the carrier thermal conductivity (κ_{el}) and the lattice thermal conductivity (κ_{lat}), expressed as

$$\kappa_{tot} = \kappa_{lat} + \kappa_{el}, \tag{4}$$

where the carrier thermal conductivity follows the Wiedemann–Franz law

$$\kappa_{el} = L_0 \sigma T, \tag{5}$$

where L_0 is the Lorenz number, σ is the electrical conductivity of the material, and T is the absolute temperature.[29] As shown in Figs. 5(a) and 5(b), both the total thermal conductivity and lattice thermal conductivity of all samples decrease monotonically with increasing temperature, which is charac-

teristic of thermal transport in crystalline materials dominated by phonon–phonon Umklapp scattering. With increasing Se content in the S/Se double-filled system, the thermal conductivity of the samples increases. Among them, the sample with $x = 0.025$ ($S_{0.075}Se_{0.025}Fe_{0.2}Co_{3.8}Sb_{12}$) exhibits the lowest total thermal conductivity of 2.07 $W{\cdot}m^{-1}K^{-1}$ at 773 K.

To clarify the impact of S/Se co-filling combined with Fe substitution on thermal transport properties more clearly, we performed fitting based on the Debye–Callaway model. The lattice thermal conductivity of the $S_{0.075}Se_{0.025}Fe_{0.2}Co_{3.8}Sb_{12}$ sample was calculated and fitted, as shown in Figs. 5(c) and 5(d). The lattice thermal conductivity of the material can be expressed by the Debye model as follows:[30,31]

$$\kappa_{\rm lat} = \frac{k_{\rm B}}{2\pi^2 v_{\rm s}}\left(\frac{k_{\rm B}T}{\hbar}\right)^3 \int_0^{\theta_{\rm D}/T} \frac{x^4 {\rm e}^x}{\tau_{\rm c}^{-1}({\rm e}^x-1)^2}\,{\rm d}x, \tag{6}$$

where $x = \hbar\omega/k_{\rm B}T$, ω is the phonon frequency, $\theta_{\rm D}$ is the Debye temperature, $\tau_{\rm c}$ is the relaxation time, $k_{\rm B}$ is the Boltzmann constant, and $\hbar$ is the reduced Planck constant. In this model, the lattice thermal conductivity primarily depends on the total phonon relaxation time, which is defined as follows:[32]

$$\tau_{\rm c}^{-1} = \frac{v}{L} + A\omega^4 + B\omega^2 T^n \exp\left(\frac{\theta_{\rm D}}{3T}\right) + C\frac{\omega^2}{(\omega^2-\omega_0^2)^2}, \tag{7}$$

where L designates the grain size, ω_0 serves as the resonant frequency, and A, B, and C correspond to the fitting parameters. The terms in the equation, from left to right, represent the contributions from grain boundary scattering (B), point defect scattering (PD), phonon–phonon scattering (U), and resonant scattering (R), respectively. For skutterudite materials, the Debye temperature is typically adopted as 287 K, and the sound velocity is taken as 2700 ms^{-1}. The corresponding fitting parameters are listed in Table 1.[31] As shown in Fig. 5(c), the experimental lattice thermal conductivity of the $S_{0.075}Se_{0.025}Fe_{0.2}Co_{3.8}Sb_{12}$ sample (red circles) shows good agreement with the fit from the Debye model (green line), indicating that the lattice thermal conductivity of the sample is governed by a combination of multiple scattering mechanisms. The fitted resonance frequencies for S and Se are obtained as 43.96 cm^{-1} and 35 cm^{-1}, respectively. To better quantify the contribution of each scattering mechanism to the reduction in lattice thermal conductivity, the spectral lattice thermal conductivity ($\kappa_{\rm s}$) arising from different scattering processes was calculated for the $S_{0.075}Se_{0.025}Fe_{0.2}Co_{3.8}Sb_{12}$ sample prepared at 3.0 GPa. Its expression is given as follows:[33]

$$\kappa_{\rm s} = \frac{k_{\rm B}}{2\pi^2 v}\left(\frac{k_{\rm B}T}{\hbar}\right)^3 \frac{x^4 {\rm e}^x}{({\rm e}^x-1)^2}\tau. \tag{8}$$

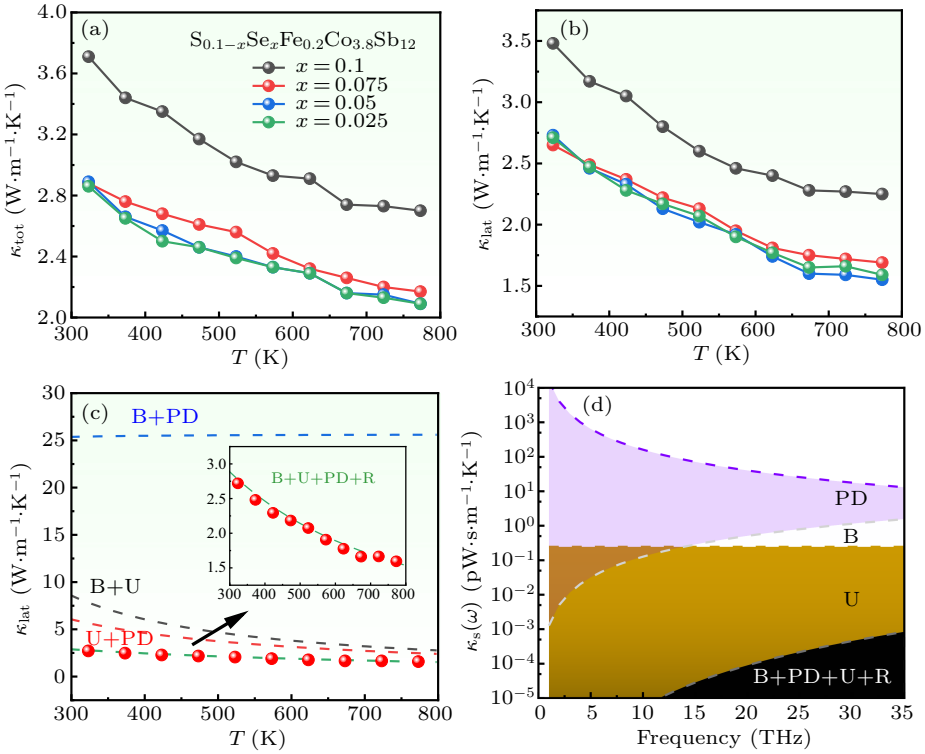


Fig. 5. Thermal properties of S/Se double filled Fe substituted skutterudite samples: (a) total thermal conductivity, (b) lattice thermal conductivity, (c) $\kappa_{\rm lat}$ experimental values of $S_{0.075}Se_{0.025}Fe_{0.2}Co_{3.8}Sb_{12}$ sample compared with the predicted $\kappa_{\rm lat}$ curve determined by Debye model and (d) calculated $\kappa_{\rm s}$ of $S_{0.075}Se_{0.025}Fe_{0.2}Co_{3.8}Sb_{12}$ sample with different scattering mechanisms prepared at 3.0 GPa.

As shown in Fig. 5(d), U dominates the low-frequency region (< 10 THz) and serves as the fundamental mechanism suppressing lattice thermal conductivity. In the mid-to-low frequency range (5–20 THz), the effect of grain B gradually weakens with increasing frequency. In the high-frequency region (> 20 THz), PD exhibits absolute dom-

inance, serving as the primary scattering source for high-frequency phonons. The sum of all scattering mechanisms (B+PD+U+R) provides full spectral coverage, manifesting the multiscale phonon scattering network constructed by the dual-filling of S/Se and Fe substitution.

Table 1. Parameters related to the calculation of lattice thermal conductivity using the Debye model.[31]

Parameter	Numerical value
Debye temperature	287 K
Longitudinal wave velocity	3850 ms^{-1}
Shear wave velocity	2450 ms^{-1}
Average sound velocity	2700 ms^{-1}
Average grain size	1.3159×10^{-6} m
Atomic volume	7.5273×10^{-28} m^3
Poisson's ratio	0.17
S resonance frequency	43.96 cm^{-1}
Se resonance frequency	35 cm^{-1}

Figure 6 shows the temperature dependence of the zT for S/Se double-filled Fe-substituted skutterudite samples synthesized at 3.0 GPa. As shown in the figure, the zT values of all samples exhibit a non-monotonic trend over the entire measured temperature range, first increasing and then decreasing with rising temperature. This trend is mainly governed by the temperature-dependent behavior of the power factor (PF $= \sigma S^2$). Among them, the $S_{0.075}Se_{0.025}Fe_{0.2}Co_{3.8}Sb_{12}$ sample achieves a peak zT of 0.22 at 673.15 K, which is significantly higher than that of other samples in most of the measured temperature range. This result not only reveals the synergistic regulation mechanism of S/Se double filling on thermoelectric properties under high-pressure synthesis, but also further expands the research direction of p-type skutterudite materials.

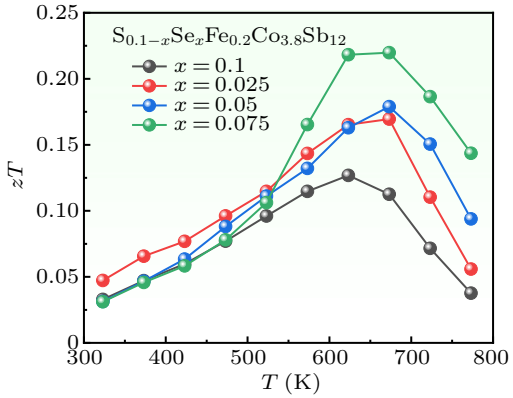


Fig. 6. The zT as a function of temperature for $S_{0.1-x}Se_xFe_{0.2}Co_{3.8}Sb_{12}$ samples with $x = 0.025$, 0.05, 0.075, and 0.1.

4. Conclusion

In summary, a series of p-type S/Se co-filled and Fe-substituted skutterudites $S_{0.1-x}Se_xFe_{0.2}Co_{3.8}Sb_{12}$ was rapidly synthesized by the HPHT method. All samples present a pure skutterudite phase. The S/Se filling ratio effectively regulates grain morphology and size by affecting atomic diffusion during HPHT processing. Fe substitution at Co sites stabilizes p-type conduction, while the S/Se ratio tunes the electrical transport properties. Meanwhile, dual anion filling introduces strong multiscale phonon scattering, resulting in significantly suppressed lattice thermal conductivity. Debye–Callaway fitting confirms that grain boundary, point defect, Umklapp, and resonant scattering act synergistically to reduce thermal transport. The optimal sample $S_{0.075}Se_{0.025}Fe_{0.2}Co_{3.8}Sb_{12}$ achieves a maximum zT of 0.22 at 673.15 K. This work provides a feasible strategy for designing electronegative-filled p-type skutterudites via HPHT, offering new insights for optimizing thermoelectric performance.

Acknowledgements

Project supported by the Natural Science Priority Foundation of Heilongjiang Province (Grant No. ZL2024E014), the Heilongjiang Provincial Department of Education Project (Grant No. 1455MNUZX001), and the Key R&D Program Project of Mudanjiang City (Grant No. XDHD25AR013).

References

[1] Shi X, Chen L and Uher C 2016 *Int. Mater. Rev.* **61** 379
[2] Nan Y, Han Y, Shen W, Zhang Z, Fang C, Wang Q, Wan B, Chen L and Zhang Y 2026 *Appl. Phys. Lett.* **128** 113905
[3] He J, Kanatzidis M G and Dravid V P 2013 *Materials Today* **16** 166
[4] Feldman J L, Singh D J, Kendziora C, Mandrus D and Sales B C 2003 *Phys. Rev. B* **68** 094301
[5] Lu G Q, Nygren E, Aziz M J, Turnbull D and White C W 1990 *Appl. Phys. Lett.* **56** 137
[6] Li X, Zhang Q, Kang Y, Chen C, Zhang L, Yu D, Tian Y and Xu B 2016 *J. Alloys Compd.* **677** 61
[7] Mona Y, Hayashi J I, Kawamura Y, Kihou K, Nishiate H, Lee C H and Sekine C 2018 *Jpn. J. Appl. Phys.* **57** 125506
[8] Fan X, Tian X, Chi J, Zhao J, Zheng Y, Wang F, Zhang L, Chen Q and Ma H 2025 *J. Eur. Ceram. Soc.* **45** 117291
[9] Chen Y, Kawamura Y, Hayashi J and Sekine C 2015 *Jpn. J. Appl. Phys.* **54** 055501
[10] Rogl G, Grytsiv A, Rogl P, Peranio N, Bauer E, Zehetbauer M and Eibl O 2014 *Acta Mater.* **63** 30
[11] Chen C, Zhang L, Li J, Yu F, Yu D, Tian Y and Xu B 2017 *J. Alloys Compd.* **699** 751
[12] Zhang J, Xu B, Wang L M, Yu D, Yang J, Yu F, Liu Z, He J, Wen B and Tian Y 2012 *Acta Mater.* **60** 1246
[13] Xiao C, Li J, Duan B, Yang H, Wang H, Zhou L, Li G and Zhai P 2022 *Ceram. Int.* **48** 4270
[14] Duan B, Yang J, Salvador J R, He Y, Zhao B, Wang S, Wei P, Ohuchi F S, Zhang W, Hermann R P, Gourdon O, Mao S X, Cheng Y, Wang C, Liu J, Zhai P, Tang X, Zhang Q and Yang J 2016 *Energy Environ. Sci.* **9** 2090
[15] Ortiz B R, Crawford C M, McKinney R W, Parilla P A and Toberer E S 2016 *J. Mater. Chem. A* **4** 8444
[16] Fukuoka H and Yamanaka S 2009 *Chem. Mater.* **22** 47
[17] Wang B, Fang D, Yi W, Zhao S, Li J, Li J, Zhao Y and Jin H 2021 *Ceram. Int.* **47** 17753
[18] Wan S, Qiu P, Huang X, Song Q, Bai S, Shi X and Chen L 2017 *ACS Appl. Mater. Interfaces* **10** 625
[19] Gharleghi A and Liu C J 2014 *J. Alloys Compd.* **592** 277
[20] Jin D, Ruan Z, Duan B, Li J, Zhai P, Yang H, Wang H, Li G and Zhou L 2021 *J. Eur. Ceram. Soc.* **41** 4484
[21] Kong L, Jia X, Sun H, Zhang Y, Sun B, Liu B, Liu H, Liu B and Ma H 2017 *J. Alloys Compd.* **697** 257

[22] Chetty R, Tobola J, Klimczyk P, Jaworska L and Wojciechowski K T 2019 *J. Alloys Compd.* **809** 151477
[23] Huang X G, Li J L, Ma H Q, Li C L, Liu T L, Duan B, Zhai P C and Li G D 2024 *Chin. Phys. Lett.* **41** 077102
[24] Humphreys J, Rohrer G S and Rollett A 2017 *Recrystallization and Related Annealing Phenomena* pp. 145–197
[25] Fan X, Gao S, Chen Q, Zhou D, Chang L, Wang Y, Zhang Y, Deng L, Ma H and Jia X 2022 *Inorg. Chem.* **61** 8144
[26] Liu W, Zhang B, Li J, Zhang H and Zhao L 2007 *J. Appl. Phys.* **102** 103717
[27] Jin M, Shi X, Feng T, Liu W, Feng H, Pantelides S T, Jiang J, Chen Y, Du Y, Zou J and Chen Z G 2019 *ACS Appl. Mater. Interfaces* **11** 8051
[28] Shi X, Wu A, Liu W, Moshwan R, Wang Y, Chen Z G and Zou J 2018 *ACS Nano* **12** 11417
[29] Kim H, Gibbs Z M, Tang Y, Wang H and Snyder G J 2015 *APL Materials* **3** 041506
[30] Callaway J 1959 *Phys. Rev.* **113** 1046
[31] Yang X H and Qin X Y 2010 *Appl. Phys. Lett.* **97** 192101
[32] Banerjee R, Chatterjee S, Ranjan M, Bhattacharya T, Mukherjee S, Jana S S, Dwivedi A and Maiti T 2020 *ACS Sustain. Chem. Eng.* **8** 17022
[33] Wu D, Xie L, Xu X and He J 2019 *Adv. Funct. Mater.* **29** 1806613